# A $Ka$-Band Indium–Antimonide Junction Circulator

Chin K. Yong, *Member, IEEE*, Robin Sloan, *Member, IEEE*, and Lionel E. Davis, *Fellow, IEEE*

***Abstract*—Following a brief overview of the underlying theory, experimental results are presented for the first time showing circulator action in a semiconductor junction structure. An axially magnetized indium–antimonide disc fixed in a three-port finline structure and cooled to the temperature of boiling nitrogen, 77 K gives circulation across $Ka$-band. For a dc magnetic bias of 0.73 T, a 15-dB isolation is recorded from 28 to 40 GHz, or a fractional bandwidth of at least 35%. Typical insertion loss is less than 1.5 dB from the WG22 reference plane at the test fixture ports. Continued operation above 40 GHz is predicted, but has not yet been measured. Measurement suggests that circulation is evident even where the effective propagation constant is imaginary, although better theoretical agreement is achieved when this is a real quantity. This new device makes millimeter-wave broad-band circulation a possibility and confirms the current model based upon the Drude–Zener approximation. A theoretical example is then given for a design operating to 140 GHz, yielding a fractional bandwidth of 110%.**

***Index Terms*—Finline, InSb, millimeter wave, semiconductor junction circulator.**

## I. Introduction

JUNCTION circulators employing ferrites have been widely studied and are well understood [1]–[4]. Ferrite designs provide good isolation, low insertion loss, and broad-band solutions at microwave frequencies. However, since the maximum saturation magnetization $(4\pi M_s)$ available is about 5500 G [5], increasing the frequency into the millimeter-wave region begets progressively narrow-band performance for ferrite junction circulators unless very high static bias fields are applied [6]. To date, the most broad-band ferrite junction circulator reported has a 10-dB isolation bandwidth of 117% between 5–19 GHz [3], [4]. This performance was achieved by extending the useful frequency into the region where the effective permeability $\mu_{\text{eff}}$ is negative, and by using a unique device configuration that assures a nearly uniform internal magnetic field. There are also millimeter-wave junction circulators that exploit the high internal anisotropy magnetic field of hexagonal ferrites [6], [7]. Although such devices have the advantage of not needing external magnets, their bandwidth is narrow. For example, the circulator reported in [6] has a 20-dB isolation bandwidth of 5%, centered at about 31 GHz.

The semiconductor junction circulator was first proposed by Davis and Sloan [8], [9]. The structure of their device is the electromagnetic dual of the ferrite circulator studied by Bosma [1]. Employing the Drude–Zener model of semiconductor and adopting the Green's function approach, a few narrow-band designs at millimeter-wave frequencies were produced. The magnetized semiconductor does not exhibit the demagnetization phenomenon experienced with the ferrite. In [9], a term representing the electron collision frequency $\nu_{\text{c}}$ was introduced into the analysis to model the losses due to electron collisions in the semiconductor. The simulated results suggested that the electron collision frequency must be small in order for the device to have low-insertion loss. Examination of these losses facilitates the choice of semiconductor for circulating action.

In later papers [10], [11], Sloan *et al.* illustrated that the semiconductor junction circulator exhibits the frequency-tracking behavior analogous to that of the ferrite circulator demonstrated by Wu and Rosenbaum [2]. By utilizing this property, millimeter-wave semiconductor junction circulators with theoretical bandwidths greater than an octave were shown to be theoretically possible. In [11], the perfect circulation conditions for the region where the effective permittivity $\varepsilon_{\text{eff}}$ is negative were presented, and it was illustrated that frequency tracking of a semiconductor junction circulator is also feasible in such a region.

In this paper, the relevant material parameters are discussed, the theory of the semiconductor junction structure is reviewed, and intriguing experimental results demonstrating such a device and confirming the validity of the Drude–Zener model are presented for the first time. A theoretical design is then presented showing circulation to 140 GHz.

## II. Permittivity Tensor of the Magnetized Semiconductor

The gyromagnetic behavior of a magnetized ferrite arises from the precessional motion of the spinning electrons. However, for a magnetized semiconductor, it is the cyclotron motion of the mobile electrons that gives rise to its gyroelectric behavior. Using the Drude–Zener model [12], [13], the tensor permittivity can be written in the form

$$[\varepsilon] = \begin{bmatrix} \xi & -j\eta & 0 \\ +j\eta & \xi & 0 \\ 0 & 0 & \zeta \end{bmatrix} \tag{1}$$

where

$$\xi = \varepsilon_{\text{r}} \left[ 1 - \frac{\omega_{\text{p}}^2(\omega - j\nu_{\text{c}})}{\omega[(\omega - j\nu_{\text{c}})^2 - \omega_{\text{c}}^2]} \right] \tag{2}$$

$$\eta = \varepsilon_{\text{r}} \left[ \frac{\omega_{\text{p}}^2 \omega_{\text{c}}}{\omega[(\omega - j\nu_{\text{c}})^2 - \omega_{\text{c}}^2]} \right] \tag{3}$$

$$\zeta = \varepsilon_{\text{r}} \left[ 1 - \frac{\omega_{\text{p}}^2}{\omega(\omega - j\nu_{\text{c}})} \right]. \tag{4}$$

The symbols $\varepsilon_o$, $[\varepsilon]$, and $\varepsilon_{\text{r}}$ denote the permittivity of free space, tensor permittivity, and static relative permittivity of the semi-

Manuscript received October 19, 1999; revised August 11, 2000.

C. K. Yong was with the University of Manchester Institute of Science and Technology, Manchester M60 1QD, U.K. He is now with the Wireless Semiconductor Division (Research and Development), Agilent Technologies Malaysia, 11900 Penang, Malaysia (e-mail: chin-kong_yong@agilent.com).

R. Sloan and L. E. Davis are with the Department of Electrical Engineering and Electronics, University of Manchester Institute of Science and Technology, Manchester, M60 1QD, U.K. (e-mail: sloan@fs5.ee.umist.ac.uk; l.davis@umist.ac.uk).

Publisher Item Identifier S 0018-9480(01)03978-3.

conductor, respectively. The symbol $\omega_{\rm p}$ denotes the plasma frequency of the semiconductor [14] and $\omega_{\rm c}$ is the cyclotron frequency defined, respectively, by

$$\omega_{\rm p} = \sqrt{\frac{e^2 N_{\rm e}}{\varepsilon_o \varepsilon_{\rm r} m_{\rm e}^*}} \tag{5}$$

$$\omega_{\rm c} = \frac{e}{m_{\rm e}^*} B_o \tag{6}$$

where $m_{\rm e}^*$ is the electron effective mass, $e$ is the electron charge, $N_{\rm e}$ is the electron concentration, and $B_o$ is the applied static magnetic field. Similar expressions were reported by Bolle and Talisa [15]. It is worth emphasizing that this Drude–Zener model is constrained by the two conditions that the cyclotron frequency must be greater than the collision frequency, i.e., $\omega_{\rm c} > \upsilon_{\rm c}$, and the effect of the holes must be negligible compared to that of the electrons. However, the inclusion of hole scattering into (4) to (6) is a relatively simple procedure provided the hole cyclotron frequency is greater than the hole scattering, i.e., $\omega_{\rm ch} > \upsilon_{\rm ch}$.

Indium antimonide (InSb) was chosen as the semiconductor due to the exceptionally high electron mobility [16]. The electron collsion frequency was calculated using (7) to be $1.69 \times 10^{11}$ s$^{-1}$, where the effective electron mass is taken to be 0.013 of the rest electron mass quoted as follows for InSb:

$$\upsilon_{\rm c} = \frac{e}{m_{\rm e}^* \mu_{\rm e}} \tag{7}$$

where $\mu_{\rm e}$ is the electron mobility of the semiconductor and was taken to be 80 m$^2$V$^{-1}$s$^{-1}$ for a pure InSb sample at 77 K [17]. Although there are several other potential candidates, such as GaAs, InSb was deemed the most suitable since its low effective electron mass allows for a manageable dc static applied magnetic field $B_0$ to achieve a high enough value of cyclotron frequency to fulfil the $\omega_{\rm c} > \upsilon_{\rm c}$ criterion. Furthermore, upon cooling to 77 K, the carrier density and, hence, plasma frequency, is shifted to an accessible part of the microwave region. InSb also possesses large $\mu_{\rm e}/\mu_{\rm h}$ and small $m_{\rm e}^*/m_{\rm h}^*$ ratios indicating that the effect due to the movement of the holes should be minimal. It is noteworthy that Suzuki [18], Suzuki and Hirota [19], May and McLeod [20], [21], White [22], and Dinger *et al.* [23] also chose the same material for their plasma semiconductor devices.

An experiment based upon the Van Der Pauw measuring technique [24], [25] was carried out to determine how $\mu_{\rm e}$ and $N_{\rm e}$ of the InSb sample vary with temperature. The results of the experiment, repeated three times, are presented in Figs. 1 and 2, respectively. The straight lines in the figures were produced by the "least-squares" best-fit method [26]. At 77 K, $\mu_{\rm e}$ and $N_{\rm e}$ of the sample are found to be 54 m$^2$V$^{-1}$s$^{-1}$ and $1.7 \times 10^{20}$ m$^{-3}$, respectively. These correspond to $\upsilon_{\rm c} = 2.51 \times 10^{11}$ s$^{-1}$ and $\omega_{\rm p} = 1.53 \times 10^{12}$ rad$^{-1}$.

## III. Review of Semiconductor Junction Circulator Theory

A schematic diagram of a semiconductor junction structure is shown in Fig. 3, and it is the electromagnetic dual of the (ideal) ferrite junction structure. Basically it is a symmetrical Y-junction of slot transmission lines with a semiconductor disc of radius $R$ inserted in the center of the junction. The peripheral areas

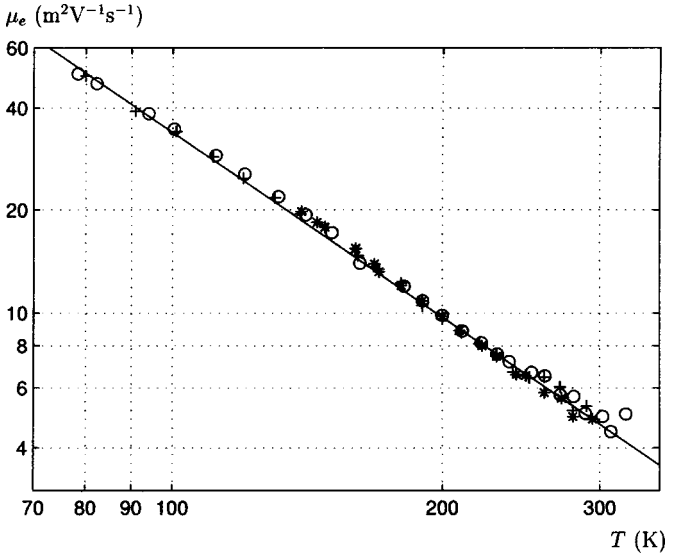


Fig. 1. Measured mobility of InSb sample versus temperature.

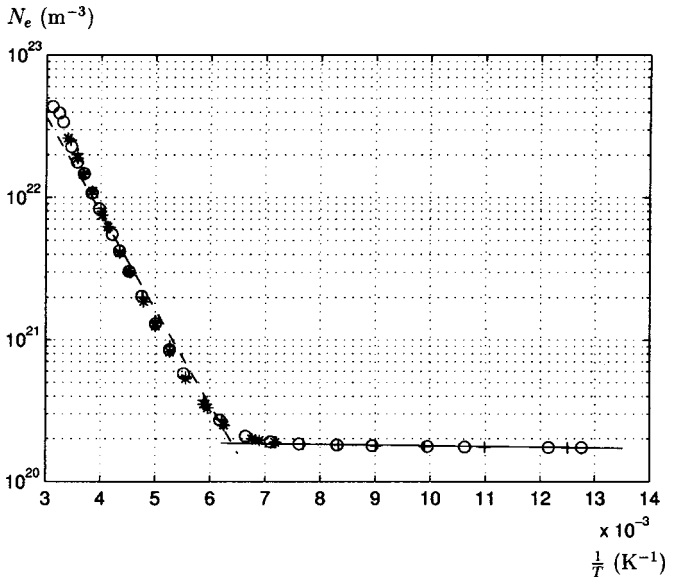


Fig. 2. Measured electron concentration in the InSb sample versus temperature.

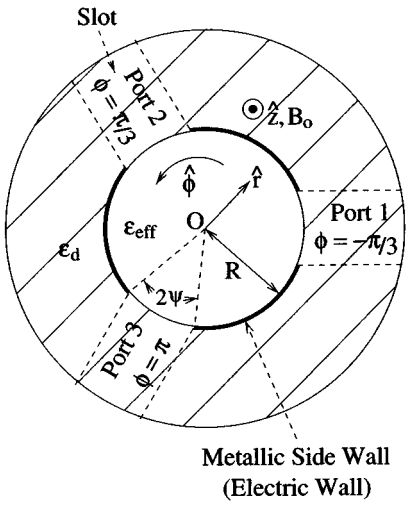


Fig. 3. Schematic diagram of the semiconductor junction circulator.

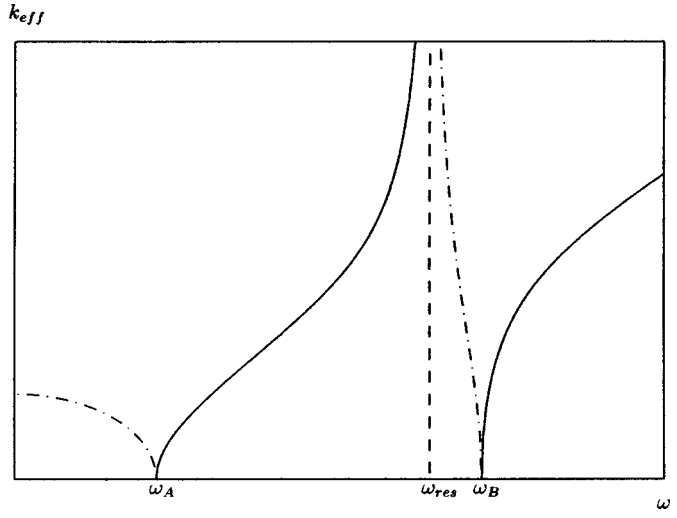


Fig. 4. Effective propagation constant versus frequency.

of the disc connected to the transmission lines are referred to as ports. Each of the ports subtends an angle of $2\psi$ with the center of the disc, where $\psi$ is referred to as the coupling half-angle of the device. Other than the port areas, the sidewall is coated with metal to provide an electric wall boundary condition. The top and bottom walls of the disc are left uncovered, giving an air–semiconductor interface. The disc is axially magnetized by a uniform and steady magnetic field of flux density $B_o$, giving rise to an effective permittivity $\varepsilon_{\text{eff}}$ [9], [11], which is defined by (8). A surrounding dielectric ring of relative permittivity $\varepsilon_{\text{d}}$ is also shown in Fig. 3 to permit a more general situation in which the medium external to the ports can be other than air. The effective propagation constant and the effective permittivity are given, respectively, by

$$\varepsilon_{\text{eff}} = \frac{\xi^2 - \eta^2}{\xi} \tag{8}$$

and

$$k_{\text{eff}} = \omega\sqrt{\mu\varepsilon_o\varepsilon_{\text{eff}}}. \tag{9}$$

It is assumed that the disc is thin enough to preclude any field variation in the $z$-direction and that only the TE modes (that give rise to nonreciprocity) are of interest.

Ignoring losses due to electron collisions $\upsilon_{\text{c}} = 0$, the effective permittivity is real and can either be positive or negative [9], [11]. As a result $k_{\text{eff}}$, calculated using (9), will either be purely real or imaginary, as illustrated in Fig. 4. The concepts of $\omega_A$, $\omega_B$, and $\omega_{\text{res}}$, shown in this figure, were discussed in [9], where $\omega_A$ and $\omega_B$ are the frequencies when the magnitude of the gyrotropic ratio $\eta/\xi$ is unity and $\omega_{\text{res}}$ is the extraordinary wave resonance frequency. Note that at frequencies below $\omega_A$, and at those between $\omega_{\text{res}}$ and $\omega_B$, $k_{\text{eff}}$ is imaginary.

A two-dimensional (2-D) Green's function was used bearing strong similarities with that of Bosma's ferrite analysis [1]. Applying the simplified boundary condition in which the electric field in the $\phi$-direction is constant over each port and zero elsewhere at the periphery, the reflection and insertion losses and the isolation of the device were derived. The derivations and expressions of these coefficients were given in [8] and [9] for the case where $k_{\text{eff}}$ is a real number and in [11] for the case where $k_{\text{eff}}$ is imaginary. The solution for the former case involves Bessel functions, while the latter involves modified Bessel functions. A more general solution including the losses due to electron collisions has also been derived using the expressions in (2) and (3) [9]. In this instance $k_{\text{eff}}$ will be complex and, thus, in general, the argument of the Bessel functions $k_{\text{eff}}R$ will be complex. This is useful for evaluating the insertion loss due to electron collisions alone.

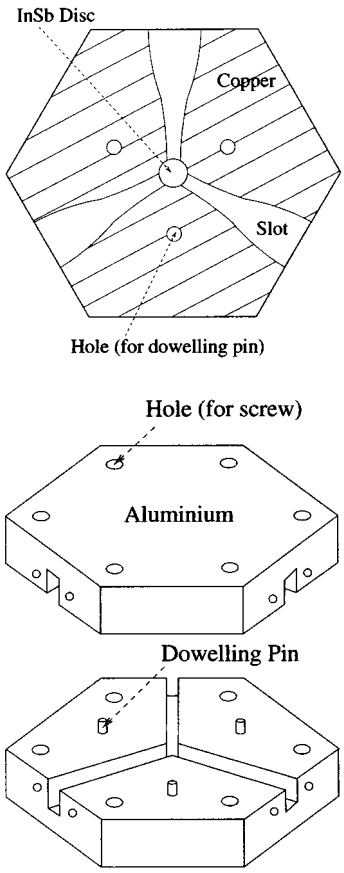


Fig. 5. Schematic diagram of the WG22 finline components.

The perfect circulation conditions (ignoring electron collisions) were derived and have been presented [11]. These are the conditions for a transmitted signal at one port to be zero. In the region where $0 \leq |\eta/\xi| \leq 1$, $k_{\text{eff}}$ is real, and where $|\eta/\xi| > 1$, $k_{\text{eff}}$ is imaginary. In [11], it was also shown that by judicious choice of the disc dimensions, coupling half-angle and the dielectric constant of the surrounding medium, the device curves of the semiconductor junction circulator can be adjusted to track the perfect circulation conditions over a wide range of $\eta/\xi$.

## IV. Experimental Results for a 30–40-GHz Design

In order to validate the theory, a design was developed to operate within the 30–40-GHz frequency range in WG22 with a finline insert and without a dielectric matching section between the air and semiconductor. A frequency range lower than that of the previous theoretical design was selected to obtain larger physical dimensions, thus enabling easier fabrication and experimental convenience, but at the expense of a larger applied field. With this design $\psi = 0.07$ rad, $R = 1$ mm, and $B_o = 0.73$ T.

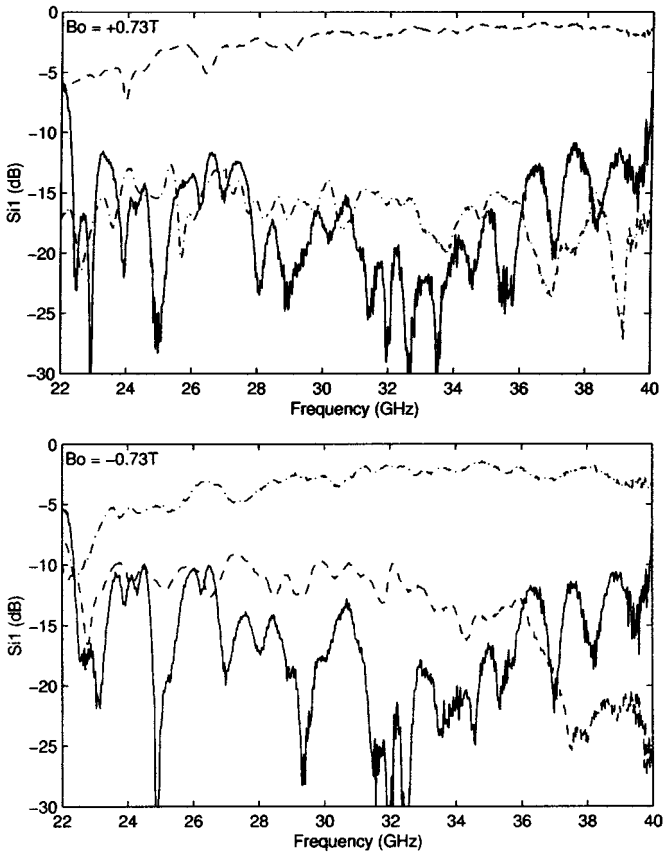


Fig. 6. Measured performance of the InSb-junction circulator at 77 K.

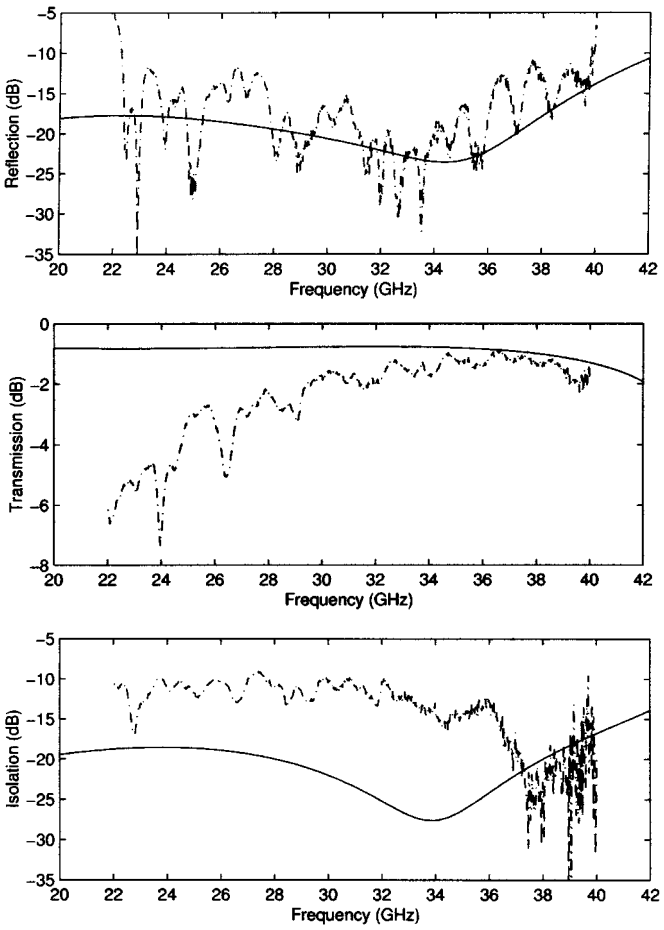


Fig. 7. Comparison of theoretical and measured results for the InSb-junction circulator at 77 K.

The schematic diagram of the circulator implemented in finline transmission line is shown in Fig. 5 using a finline circular-arc taper design in WG22 discussed by Beyer and Wolff [27].

An HP8510 network analyzer with thru-reflection line (TRL) calibration implemented at the end of the WG22 waveguide ports was used to measure the $S$-parameter responses of the circulator, and the results are presented in Fig. 6 for $B_0 = \pm 0.73$ T. From this figure, the isolation is at least 10 dB in the 22–40-GHz range, but goes to nearly 25 dB at 36.5–40-GHz frequencies for $B_0 = -0.73$ T. The minimum insertion loss is about 1 dB in the 34–38-GHz range for $B_0 = +0.73$ T. It is expected that further reduction in the insertion loss is possible if appropriate matching networks are incorporated at the ports to minimize the reflection. The results also suggest that circulation continues beyond the current measurement window. It is also worth noticing that circulation is reversed, just like the case of the ferrite circulator, when the magnetic field is applied in the opposite direction. Discrepancies in the measured $S$-parameters between the two dc magnetic bias directions can be attributed to unintentional asymmetries caused in construction. The ripple associated with the measured response could be further reduced by using a TRL calibration in the finline, thus moving the measurement reference plane up to the ports of the semiconductor junction circulator.

The comparisons between the experimental results of the InSb-junction circulator at 77 K and their theoretical responses are presented in Fig. 7. It can be seen that, for the reflection coefficient, the measurement and theoretical values are in reasonable agreement. For the transmission coefficient, the measured response is quite close to predicted values for the 34–40-GHz frequency range, but deteriorates with decreasing frequency. For the isolation response, the measurement is similar in shape to that predicted, but with closest agreement and best performance in isolation for the frequency region from around 34–40 GHz. The results also suggest that the circulator has less isolation capability in practice, particularly at frequencies below 37 GHz. It is also worth pointing out that 37 GHz corresponds to the $\omega_A$ frequency below which $k_{\text{eff}}$ is imaginary in this case. For more accurate performance predictions, a three-dimensional model will be necessary. The current 2-D model assumes the electromagnetic fields are confined solely to the InSb disc. In practice, the boundary step between the air and semiconductor where the wave penetration into the semiconductor is evanescent due to the imaginary $k_{\text{eff}}$ will have an effect.

## V. Broad-Band Theoretical Millimeter-Wave Circulator

Given that the theory developed has now been confirmed experimentally, a millimeter-wave InSb-junction circulator operating at 77 K has been designed having $B_o = 0.35$ T, $\psi = 0.5$ rad, $R = 0.24$ mm, and $\varepsilon_{\text{d}} = 20$. Cooling is necessary

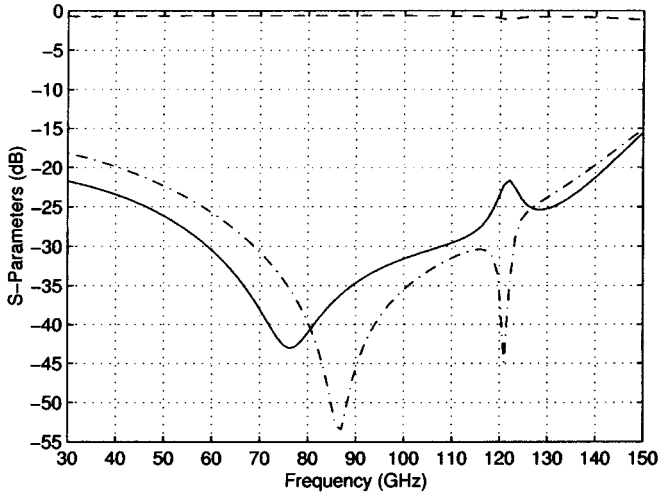


Fig. 8. Predicted broad-band $S$-parameter response for the InSb-junction circulator at 77 K.

in order to maximize electron mobility and to provide the desired carrier density. Note that the magnitude of the magnetic dc bias is comparable to that of ferrite junction circulators. As illustrated in the theoretical responses of Fig. 8, the InSb circulator has a 20-dB-isolation relative bandwidth of 111%, and an insertion loss due to electron collisions that varies from 0.7 to 1.1 dB in the frequency range of 40–140 GHz. (Conductor losses due to the metal applied at the disc edge have not been included in the calculation.) This bandwidth far exceeds that of simulated ferrite circulators in the same frequency range. This design was formulated using the measured results from the Van Der Pauw technique for the InSb sample $N_{\rm e} = 1.7 \times 10^{20}$ m$^{-3}$, $\upsilon_{\rm c} = 2.51 \times 10^{11}$ s$^{-1}$ at 77 K, and $m_{\rm e}^* = 0.013 m_o$, where $m_o$ is the free electron mass and $\varepsilon_{\rm r} = 17.7$ [16].

## VI. Conclusion

Operation of the semiconductor junction circulator has been demonstrated for the first time. An InSb disc of radius 1 mm, cooled to boiling nitrogen temperature, placed in a finline three-port structure and with an applied axial dc magnetic bias of $+0.73$ T yielded 15-dB isolation between 28–40 GHz. Insertion loss was better than 1.5 dB over the measured 32–40-GHz frequency range from the reference plane at entry to the three-port jig. It is likely that the usable frequency range extends beyond 40 GHz—this being the upper frequency limit of the measurement system. This is an impressive result confirming approximate theory based upon the Drude–Zener model incorporated in the 2-D Green's function. Circulating action has also been measured in the frequency range where the axial propagation coefficient is imaginary, i.e., below 37 GHz, although measurement and theory correlate less well for this region. Extending the model to three dimensions should improve the accuracy and, hence, circulator design, particularly for frequencies below $\omega_A$. Perhaps the most tantalizing feature of these results is the uncertainty in the performance of this new device above 40 GHz. A review of the relevant material properties of a semiconductor for use as a circulator is presented, as well as a theoretical design, illustrating the potentially enormous bandwidth of operation.

## Acknowledgment

The authors would like to thank K. Singer, UMIST, Manchester, U.K., for his assistance and advice in the semiconductor characterization measurements and Wafer Technology Ltd., Milton Keynes, U.K., for the provision of the InSb wafer. The author also thank N. Priestley, EEV Ltd., Lincoln, U.K., for the fabrication of the InSb discs.

## References

[1] H. Bosma, "On stripline Y-circulator at UHF," *IEEE Trans. Microwave Theory Tech.*, vol. MTT-12, pp. 61–72, Jan. 1964.
[2] Y. S. Wu and F. J. Rosenbaum, "Wide-band operation of microstrip circulators," *IEEE Trans. Microwave Theory Tech.*, vol. MTT-22, pp. 849–856, Oct. 1974.
[3] E. F. Schloemann and R. E. Blight, "Broad-band stripline circulators based on YIG and Li-ferrite single crystals," *IEEE Trans. Microwave Theory Tech.*, vol. MTT-34, pp. 1394–1400, Dec. 1986.
[4] E. F. Schloemann, "Circulators for microwave and millimeter-wave integrated circuits," *Proc. IEEE*, vol. 76, pp. 188–200, Feb. 1988.
[5] W. H. Von Aulock, *Handbook of Microwave Ferrite Materials*. New York: Academic, 1965.
[6] J. A. Weiss, N. G. Watson, and G. F. Dionne, "New uniaxial-ferrite millimeter-wave junction circulators," in *IEEE MTT-S Int. Microwave Symp. Dig.*, vol. 1, June 1989, pp. 145–148.
[7] Y. Akaiwa and T. Okazaki, "An application of a hexagonal ferrite to a millimeter-wave Y circulator," *IEEE Trans. Magn.*, vol. MAG-10, pp. 374–378, June 1974.
[8] L. E. Davis and R. Sloan, "Semiconductor junction circulators," in *IEEE Int. Microwave Symp. Dig.*, vol. 1, June 1993, pp. 483–486.
[9] ——, "Predicted performance of semiconductor junction circulators with losses," *IEEE Trans. Microwave Theory Tech.*, vol. 41, pp. 2243–2247, Dec. 1993.
[10] R. Sloan, C. K. Yong, and L. E. Davis, "Broad-band millimetric semiconductor junction circulators At 77 K," in *IEEE Int. Microwave Symp. Dig.*, vol. 1, June 1996, pp. 109–112.
[11] ——, "Broad-band theoretical gyroelectric junction circulator tracking behavior at 77 K," *IEEE Trans. Microwave Theory Tech.*, vol. 44, pp. 2655–2660, Dec. 1996.
[12] R. R. Rau and M. E. Caspari, "Faraday effect in germanium at room temperature," *Phys. Rev.*, vol. 100, pp. 632–639, Oct. 1955.
[13] C. Cavalli, J.-L. Amalric, and H. Baudrand, "Various aspects of nonreciprocal devices using magnetised semiconductors," *Proc. Inst. Elect. Eng.*, pt. H, vol. 140, pp. 165–172, June 1993.
[14] B. Lax, "Magnetoplasma effects in solids," *IRE Trans. Microwave Theory Tech.*, vol. MTT-9, pp. 83–89, Jan. 1961.
[15] D. M. Bolle and S. H. Talisa, "Fundamental considerations in millimeter and near-millimeter component design employing magnetoplasmons," *IEEE Trans. Microwave Theory Tech.*, vol. MTT-29, pp. 916–923, Sept. 1981.
[16] S. M. Sze, *Physics of Semiconductor Devices*, 2nd ed. New York: Wiley, 1981, pp. 850–851.
[17] O. Madelung, Ed., *Semiconductors, Physics of Group IV and Elements and III–V Compounds*. Berlin, Germany: Springer-Verlag, 1982, vol. 17a.
[18] K. Suzuki, "Room temperature solid-state plasma nonreciprocal microwave devices," *IEEE Trans. Electron Devices*, vol. ED-16, pp. 1018–1021, Dec. 1969.
[19] K. Suzuki and R. Hirota, "Nonreciprocal millimeter-wave devices using a solid-state plasma at room temperature," *IEEE Trans. Electron Devices*, vol. ED-18, pp. 408–411, July 1971.
[20] W. G. May and B. R. McLeod, "A waveguide isolator using InSb," *IEEE Trans. Microwave Theory Tech.*, vol. MTT-16, pp. 877–878, Oct. 1968.
[21] B. R. McLeod and W. G. May, "A 35-GHz isolator using coaxial solid-state plasma in a longitudinal magnetic field," *IEEE Trans. Microwave Theory Tech.*, vol. MTT-19, pp. 510–516, June 1971.
[22] D. J. White, "Room-temperature Faraday rotation in n-type InSb films at 23.4 GHz," *J. Appl. Phys.*, vol. 39, pp. 5083–5086, Oct. 1968.

[23] R. J. Dinger, T. M. Waugh, and D. J. White, "Nonreciprocal properties of vacuum-deposited InSb films at 87 GHz," *IEEE Trans. Microwave Theory Tech.*, vol. MTT-22, pp. 879–880, Oct. 1974.
[24] L. J. Van Der Pauw, "A method of measuring specific resistivity and Hall effect of discs of arbitrary shape," *Philips Res. Rep.*, vol. 13, pp. 1–9, Feb. 1958.
[25] ——, "A method of measuring the resistivity and Hall coefficient on lamellae of arbitrary shape," *Philips Tech. Rev.*, vol. 20, pp. 220–224, Mar. 1959.
[26] S. L. Meyer, *Data Analysis for Scientists and Engineers*. New York: Wiley, 1975, pp. 850–851.
[27] A. Beyer and I. Wolff, "Finline taper design made easy," in *IEEE Int. Microwave Symp. Dig.*, June 1985, pp. 493–496.

**Chin K. Yong** (M'99) was born in Muar, Johor, Malaysia, in 1970. He received the B.Eng. degree in electronic and optoelectronic engineering, M.Sc. degree, and Ph.D. degree in microwave engineering from the University of Manchester Institute of Science and Technology (UMIST), Manchester, U.K., in 1994, 1996, and 1999, respectively.

During his postgraduate studies, he was mainly engaged in gyrotropic components. In 1999, he joined the Wireless Semiconductor Division (Research and Development), Agilent Technologies Malaysia, Penang, Malaysia, where he is currently engaging in analog integrated-circuit (IC) design.

Dr. Yong was the recipient of the IEEE Microwave Theory and Techniques Society (IEEE MTT-S) Graduate Fellowship in 1997.

**Robin Sloan** (M'92) received the B.Sc. (with honors) degree in electronic engineering from Sussex University, Sussex, U.K., in 1985, and the M.Sc. and Ph.D. degrees from the University of Manchester Institute of Science and Technology (UMIST), Manchester, U.K., in 1988 and 1990, respectively.

From 1985 to 1987, he was with the Seeker Systems Group, British Aerospace Air Weapons Division. From 1991 to 1992, he was with Milmega Ltd., Isle of Wight, U.K., where he was involved with stripline power combiners and dividers, power amplifiers, and grid modulators for traveling wave tubes (TWTs). Following a one-year appointment as a Research Associate at UMIST, he was with the Ferranti Satellite Communications Division, Stockport, U.K., where he was involved with dielectric-resonator oscillators and power amplifiers. In 1993, he became a Lecturer in the Department of Electrical Engineering and Electronics, UMIST, and a Senior Lecturer in 1999. His teaching interests are electromagnetics and microwave circuit design and his current research interests are novel nonreciprocal devices, spatial power combining, and microelectromechanical systems (MEMs).

**Lionel E. Davis** (F'95) received the B.Sc. degree from the University of Nottingham, Nottingham, U.K., in 1956, and the Ph.D. degree from the University of London, London, U.K., in 1960.

From 1959 to 1964, he was with Mullard Research Laboratories, Redhill, U.K. From 1964 to 1972, he was an Assistant Professor and then an Associate Professor of electrical engineering from Rice University, Houston, TX. From 1972 to 1987, he was with Paisley College, Paisley, Scotland, where he was a Professor and Head of the Department of Electrical and Electronic Engineering. In 1987, he joined the University of Manchester Institute of Science and Technology (UMIST), Manchester, U.K., where he is currently a Professor of communication engineering. He was a Visiting Professor at the University College London, London, U.K., and the University of California at San Diego, La Jolla, and has been a consultant for several companies. He research has included passive components, high-$T_c$ superconductors, and dielectric-resonator antennas and chiral materials. His current research interests are in gyrotropic media and nonreciprocal components for microwave, millimeter-wave, and optical wavelengths.

Dr. Davis is a Fellow of the Institution of Electrical Engineers (IEE), U.K. and the Institute of Physics. He is a member of the IEEE Microwave Theory and Techniques Society (IEEE MTT-S) International Microwave Symposium (IMS) Technical Programme Committee and co-chairman of the IEEE MTT-S Committee on Microwave Ferrites. He was a founding member of the Houston Chapter of the IEEE MTT-S. He has served on the Council, the Microwave Theory and Devices Committee, and the Accreditation Committee of the IEE, and is member of the Peer Review College of the Engineering and Physical Sciences Research Council.